Supplemental Data

Polycomb repressive complex 2-mediated chromatin repression guides effector CD8+ T cell terminal differentiation and loss of multipotency

Simon M. Gray[1,*,†], Robert A. Amezquita[1,*], Tianxia Guan[1], Steven H. Kleinstein[1,2,3], and Susan M. Kaech[1,†,4]

Supplemental Experimental Procedures

Infections and treatments

For primary infection, 5-6 week old mice were infected with $2x10^5$ PFU of the LCMV Armstrong strain by intra-peritoneal (i.p.) injection. Viral titers were measured by plaque assay as previously described (Ahmed et al., 1984). For challenge with secondary infection, mice were infected intravenously (i.v.) with $1x10^5$ CFU/mouse of recombinant *Listeria monocytogenes* strain XFL203 which expresses the GP_{33-41} epitope of LCMV, called LM-33 (Kaech and Ahmed, 2001). For LM-33 titers, organs were harvested and processed in antibiotic free media, then incubated with an equal volume of 1% Triton X-100 made in H_2O, and plated in dilutions on Difko Brain Heart Infusion Agar plates (Becton Dickinson). Tamoxifen purchased from Cayman Chemical (Ann Arbor, MI) was dissolved in peanut oil at 20 mg/mL and mice were orally gavaged with 100 μL (2mg) per treatment.

Gene expression by qRT-PCR and immunoblotting

RNA was isolated from 100,000 sorted cells by TRIzol extraction (Life Technologies) followed by ethanol precipitation. SSRTII (Life Technologies) was used for CDNA preparation. qRT-PCR analysis was performed with an Agilent Mx3000P qPCR system using iTaq Universal SYBR Green super mix (Bio-Rad Laboratories). Relative expression was calculated as fold change over the ribosomal gene *Rpl9 (L9)*. The following primers were used: *Bach2* forward: 5'-TGAGGTACCCACAGACACCA-3' *Bach2* reverse: 5'-TGCCAGGACTGTCTTCACTG-3'; *Foxo1* forward: 5'-TGTCAGGCTAAGAGTTAGTGAGCA-3' *Foxo1* reverse: 5'-GGGTGAAGGGCATCTTTG-3'; *Id3* forward: 5'-GACTCTGGGACCCTCTCTC-3' *Id3* reverse: 5'-ACCCAAGTTCAGTCCTTCTC-3'; *Tbet* forward: 5'-AGCAAGGACGGCGAATGTT-3' *Tbet* reverse: 5'-GTGGACATATAAGCGGTTCCC-3'; *Rpl9* forward: 5′-TGAAGAAATCTGTGGGTCG-3′ *Rpl9* reverse: 5′-GCACTACGGACATAGGAACTC-3′; *Tcf7* forward 5'-AGAAGCCAGTCATCAAGAAA-3' *Tcf7* reverse 5'-CATTTCTTTTTCCTCCTGTG-3'. Immunoblotting was performed as previously described using rabbit monoclonal antibodies from Cell Signaling: EZH2 (D2C9), β-Actin (13E5), H3K27me3 (C62B11), H3 (D1H2)(Hand et al., 2007).

Chromatin immunoprecipitation (ChIP) and ChIP-Sequencing (ChIP-Seq)

ChIP experiments were performed on FACS purified *in vivo* adoptively transferred P14^{+} CD8^{+} T cells. CD8α^{+}CD44^{+}Thy1.1^{+} cells were sorted based on expression of KLRG1 and IL7Rα to purified populations of TE (KLRG1^{Hi}IL7Rα^{Lo}) and MP (KLRG1^{Lo}IL7Rα^{Hi}) cells. Cells were crosslinked with 1% formaldehyde in 10% fetal bovine serum containing RPMI medium for 10 minutes at 37°C. Crosslinking was stopped by addition of 2.5M glycine at 1:20 dilution for 5 minutes at room temperature. Washed cells were lysed and sonicated to obtain chromatin fragments of 150 to 500 base pairs. ChIP was performed on sonicated chromatin from 1-10 million cells with anti-H3K27me3 (Abcam, ab6002) and anti-H3K27ac (Abcam, ab4729) antibodies. Immunoprecipitated DNA was purified, amplified, processed into a library, and sequenced on an Illumina HiSeq 2500 with 4 samples per lane (170M reads are distributed at 42.5M reads per sample with 75bp reads in single-end mode). The resulting fastq file from each sample was first trimmed for TruSeq adapters, and those with 5'/3' end qualities lower than 30/20 were excluded from further analysis. Reads were then aligned to the mm10 (GRCm38) reference genome using bowtie2. Alignments were then filtered to remove duplicate reads and blacklisted regions as defined by ENCODE, and visualized as bigwig files using the DeepTools bamCoverage utility. FastQC was run on both raw and processed data to assess sequencing quality. Conventional ChIP was performed with anti-mouse IgG as negative control and immunoprecipitated DNA was analyzed by qPCR as above with the following primers: *Tcf7* TSS forward: 5'-CCTTCGGACTCATTCACCAG-3' *Tcf7* TSS reverse:5'-GCGAGGAACAGGACGATAAG-3'; *Id3* TSS forward: 5'- ACTCAGCTTAGCCAGGTGGA-3' *Id3* TSS reverse: 5'- CACCTGAAGGTCGAGGATGT-3'; *Bach2* intron 1 forward: 5'- TCAGCCTTTAAGAGCCCAAA *Bach2* intron 1 reverse: 5'-AAAGGGGGACCCCTCTAAAT; *Ttn* forward: 5'- CCGCATCTTTGACACTGAGA *Ttn* reverse: 5'-AAAGGGTGACCAGGAGCTTT.

Analysis of ChIP-seq Data.

MACS2 Peak Calling. Peaks were first called for each sample using MACS2 v2.1.0, normalizing relative to input in each case. For H3K27ac, default macs2 settings were used, and for H3K27me3, the --broad setting was invoked. *Replication of Peaks.* Given that ChIP-seq samples were acquired in separate batches, and additionally since each sample possessed different IP efficiencies, a single significance threshold cutoff for peak calling proved insufficient to filter out low-quality peaks. To address this, q-value thresholds were defined for each individual sample by fitting the distribution of all candidate peak q-values to a mixture of two Gaussian distributions. The top 75% of peaks from the distribution with lower q-values were retained for further analysis. *Consensus Peaksets.* A consensus peakset was defined first for each condition based on the replicates. To accomplish this, bedtools intersect was used to capture consensus regions, followed by defining a peakset with respect to the given mark by using bedtools merge to combine these consensus

peaksets. *Annotation of Peaksets.* Regions were annotated to the nearest gene TSS using the bedtools v2.26 closest utility – for regions with one-to-many mappings for a given transcript, the most highly expressed transcript across MP and TE $CD8^+$ T cells was used to reduce annotation to be one-to-one. *Region Functional Annotation.* Gene ontology analysis of genomic regions was performed using the Stanford GREAT online tool(McLean et al., 2010).

Differential Modification Analysis

Read counts were first tallied over the consensus peaksets for each mark per sample in R using the GenomicAlignments v1.10 package's summarizeOverlaps function, ignoring strand and in union mode. Subsequently, analysis was performed DESeq2 v1.14.1, with the read counts normalized by fitting the data to a local smoothed dispersion fit to better capture the observed dispersion-mean relationship. Differential analysis was then performed to determine statistically significant differentially modified regions, defined as those with FDR (Benjamini-Hochberg) less than 0.1 and fold-change greater than 1.2. Statistical analysis and visualization of sequencing data was performed using custom R scripts.

Flow cytometry, surface and intracellular staining, peptide stimulations, and antibodies

Lymphocyte isolation, LCMV peptide stimulations, MHC class I tetramer production, and surface and intracellular staining were performed as previously described(Murali-Krishna et al., 1998). Conjugated antibodies were purchased from Biolegend: KLRG1 (2F1), IFNγ (XMG1.2), CD62L (MEL-14), CD8α (53-6.7), CD44 (IM7), Thy1.1 (OX-7), T-bet (4B10), TNFα (MP6-XT22); and eBioscience: IL7Rα (A7R34), CD27 (LG.7F9), IL-2 (JES6-5H4), Eomes (Dan11mag). Primary unconjugated rabbit monoclonal antibodies were purchased from Cell Signaling: TCF1 (C63D9), FOXO1 (C29H4), EZH2 (D2C9), and detected by anti-rabbit IgG 647 or anti-rabbit IgG 488 antibody (ThermoFisher Scientific). Foxp3/Transcription Factor Staining Buffer Set (eBioscience) was used for intracellular permeabilization. Flow cytometry was performed on an LSRII (Becton Dickinson) and analyzed with FlowJo software (FlowJo, LLC). Sorting was performed with a BD FACS Aria II (Becton Dickinson).

In vitro culture and CellTrace Violet proliferation assay

For *in vitro* cultures, $1x10^6$ naïve splenocytes were cultured with GP_{33-41} peptide, or αCD3 (1μg/ml) (Biolegend) and αCD28 (0.5 μg/ml) (Biolegend), and IL-2 (10ng/ml) (R&D Systems) for the specified time. For proliferation assays, naïve splenocytes were labeled with CellTrace Violet (ThermoFisher Scientific) according to the vendor protocol, then either cultured *in vitro* as above or adoptively transferred to recipients and infected with LCMV Armstrong as above.

Mixed bone marrow chimeras

To generate mixed bone marrow chimeras, bone marrow from Thy1.1^{+}Ly5.2^{+}EZH2$^{+/+}$ mice was mixed in a 80:20 ratio with bone marrow from Thy1.2^{+}Ly5.2^{+}*Ezh2*$^{f/f}$GzmBCre^{+} mice and used to reconstitute naïve wildtype lethally irradiated Thy1.2^{+}Ly5.1^{+} recipient mice. Two months post-reconstitution, mixed bone marrow chimeric mice were infected with LCMV-Armstrong and lymphocytes were isolated and analyzed as described above.

Retroviral overexpression

Retrovirus supernatant was produced in HEK293T cells. MSCV-empty-vector-GFP and MSCV-*T-bet*-GFP (Tbet-overexpression)(Szabo et al., 2000) were obtained from L. Glimcher (Dana Farber, Boston, MA). P14^{+} TCR transgenic mice were superinfected *i.v.* with 2x10^{6} PFU of the LCMV-Armstrong strain. 24 hours later, P14^{+} splenocytes were spin-transduced at 6 million cells per 24 well-plate well for 90 minutes at 37°C with viral supernatants from 293T cells supplemented with 8μg/mL of hexadimethrine bromide (Sigma, H9268), then 1x10^{5} P14^{+} CD8^{+} T cells were adoptively transferred to naïve B6 recipient mice that were subsequently infected with 2x10^{5} PFU of LCMV-Armstrong strain.

SUPPLEMENTAL FIGURES and SUPPLEMENTAL FIGURE LEGENDS

Figure S1. (related to Figure 1)

A

Sample ID	Subset	Factor	Condition	Replicate	Reads	Dup%	ReadL	FragL	RelCC	SSD	RiP%
K27Ac_WT_MP_d10_1	MP	K27Ac	WT	1	3501380	0	74	291	3.4	4.6	26
K27Ac_WT_MP_d10_2	MP	K27Ac	WT	2	5084646	0	74	260	3.2	1.5	6
K27Ac_WT_TE_d10_1	TE	K27Ac	WT	1	3537850	0	74	300	3.9	3.2	16
K27Ac_WT_TE_d10_2	TE	K27Ac	WT	2	4980768	0	73	282	4.3	1.1	4
K27me3_WT_MP_d10_1	MP	K27me3	WT	1	2335714	0	74	300	5.1	1.1	8
K27me3_WT_MP_d10_2	MP	K27me3	WT	2	3245666	0	74	295	3.6	1.8	3.9
K27me3_WT_TE_d10_1	TE	K27me3	WT	1	3663418	0	74	300	5.7	2.3	9.7
K27me3_WT_TE_d10_2	TE	K27me3	WT	2	3727814	0	74	300	4	1	2.1

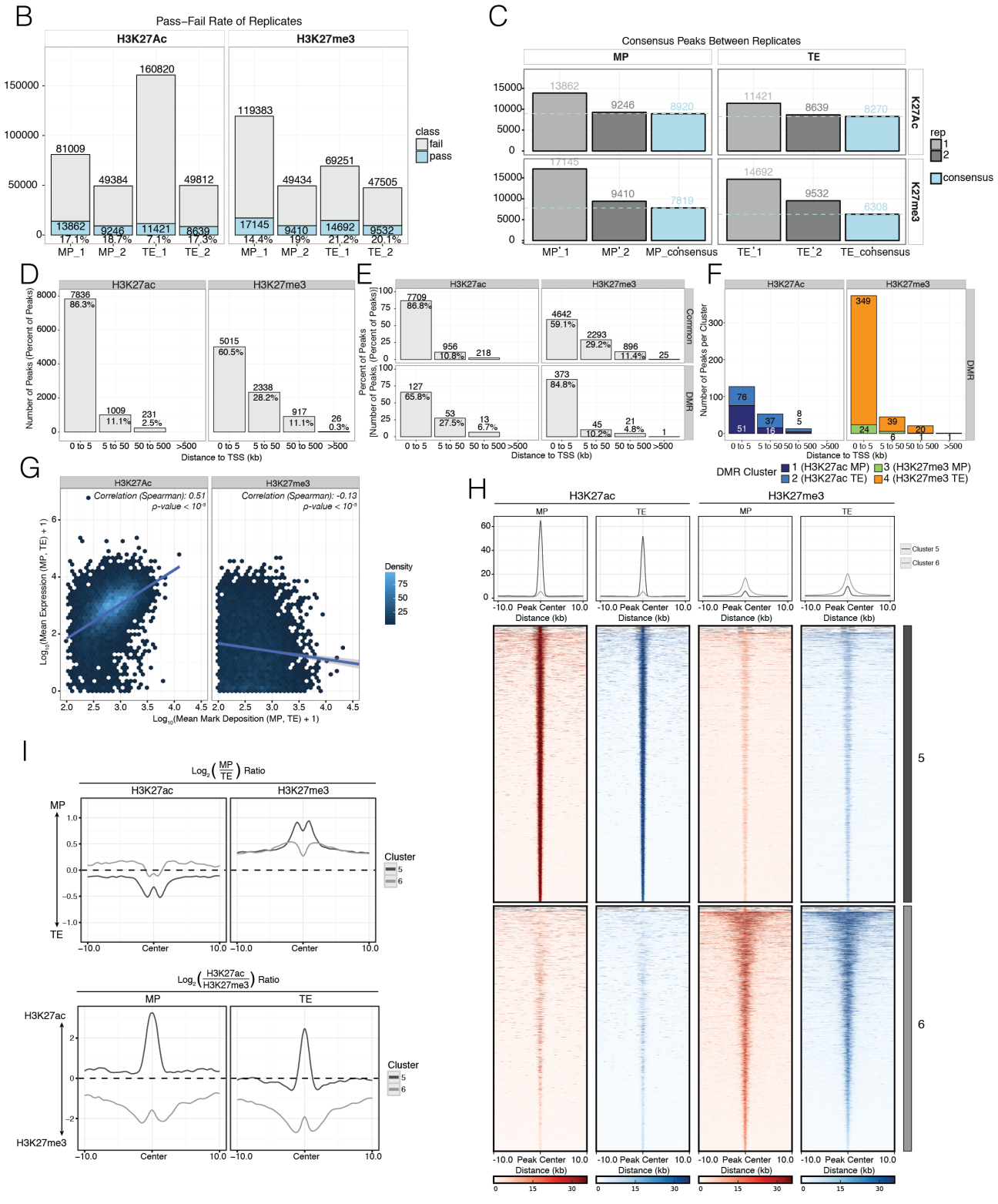

Figure S1. (related to Figure 1) Quality control and summary statistics of H3K27ac and H3K27me3 ChIP-seq in Memory Precursors and Terminal Effector cells.

A) Table summarizing quality control metrics for replicates of H3K27ac and H3K27me3 ChIP-Seq datasets following data processing. Dup% = % duplicate reads, ReadL = read length, FragL = fragment length, RelCC = relative cross-coverage score, SSD = squared sum of deviations, RiP% = % reads in peaks.

B) Stacked bar graph of quality control (QC) pass-fail rate of reads from replicates of H3K27ac and H3K27me3 ChIP-Seq datasets. Reads passing QC are in blue and reads failing QC are in gray. The percentage of reads passing QC is shown below each bar.

C) Bar graph showing the number of consensus peaks (blue) shared between replicates (light gray and dark gray) of H3K27ac and H3K27me3 ChIP-Seq datasets.

D-F) Consensus peaks were annotated to the TSS of the nearest gene. Shown are bar plots pertaining to the number of regions falling within a given distance for all H3K27ac and H3K27me3 regions (D), then separately for DMRs versus Common regions (E), and finally only for DMRs (F).

G) Scatter plot of the normalized mean deposition of H3K27ac (left) and H3K27me3 (right) across MP and TE cells versus the normalized mean gene expression in MP and TE cells, where each region was associated with the gene with the nearest TSS as shown in D-F.

H) Deposition of H3K27me3 and H3K27ac in MP and TE cells centered on Common regions +/-10kb. Common regions are defined as regions with FDR > 0.1 and/or fold-change < 1.2 in volcano plots in Fig 1A (Cluster 5) and B (Cluster 6). Line plots at top show the summary distributions across each cluster for each H3K27ac and H3K27me3 in MP and TE cells, respectively.

I) Line plots show the ratio of H3K27ac or H3K27me3 comparing MP versus TE cells for each set of Common regions in clusters 5 and 6 (top), and similarly, the ratio of H3K27ac to H3K27me3 within both MP and TE cells (bottom).

Data shown contain the union of significant consensus peaks identified across two independent biological replicates of ChIP-Seq experiments for H3K27ac and H3K27me3 (A-I; n=10-20 mice/group/replicate).

Figure S2. (related to Figure 2)

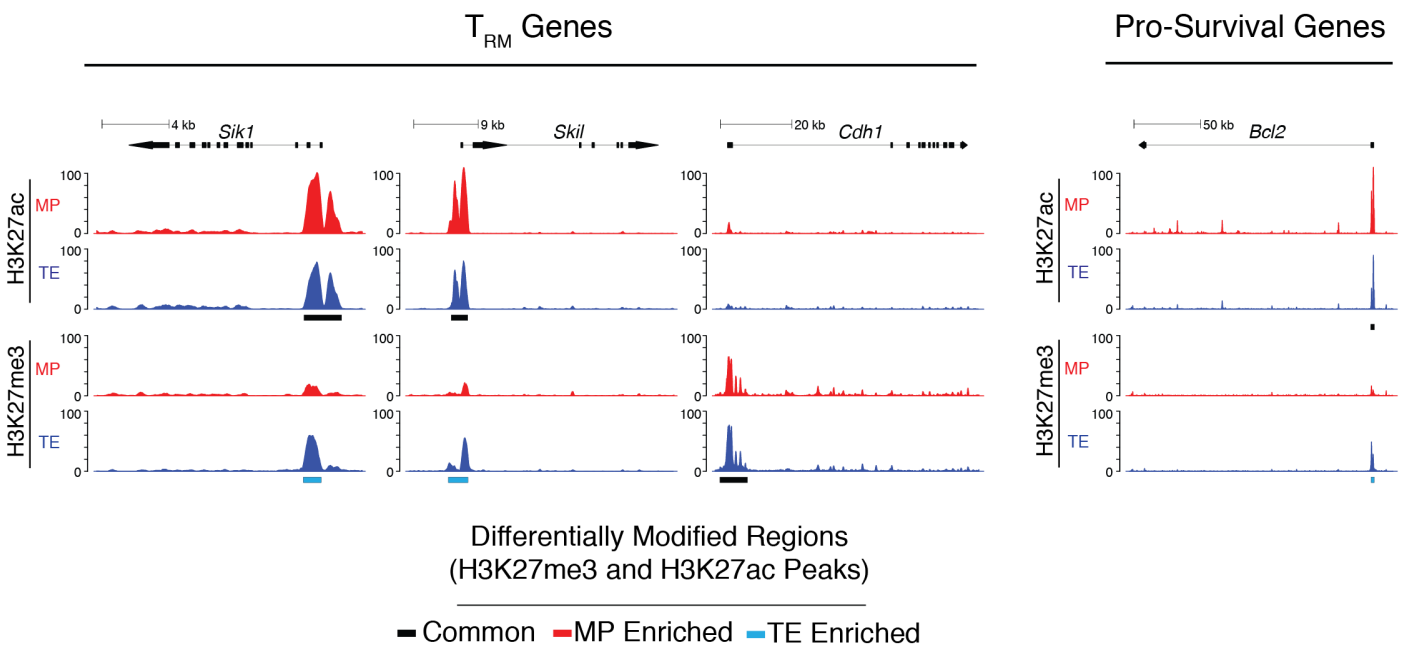

Figure S2. (related to Figure 2) T resident memory genes and Pro-survival genes exhibit substantially more H3K27me3 and less H3K27ac deposition in TE versus MP cells.

Alignment tracks of H3K27ac and H3K27me3 deposition across MP and TE cells at tissue resident memory (T_{RM}) and pro-survival genes (T_{RM} signature genes were defined by (Mackay et al., 2013)). Statistically significant differentially modified regions (DMRs) are marked by rectangles below tracks with red bars representing enrichment in MP cells and blue bars representing enrichment in TE cells. Black bars demarcate called peaks that are not enriched in one population over the other.

Data shown contain the union of significant consensus peaks identified across two independent biological replicates of ChIP-Seq experiments for H3K27ac and H3K27me3 (A-B; n=10-20 mice/group/replicate).

Figure S3. (related to Figure 4)

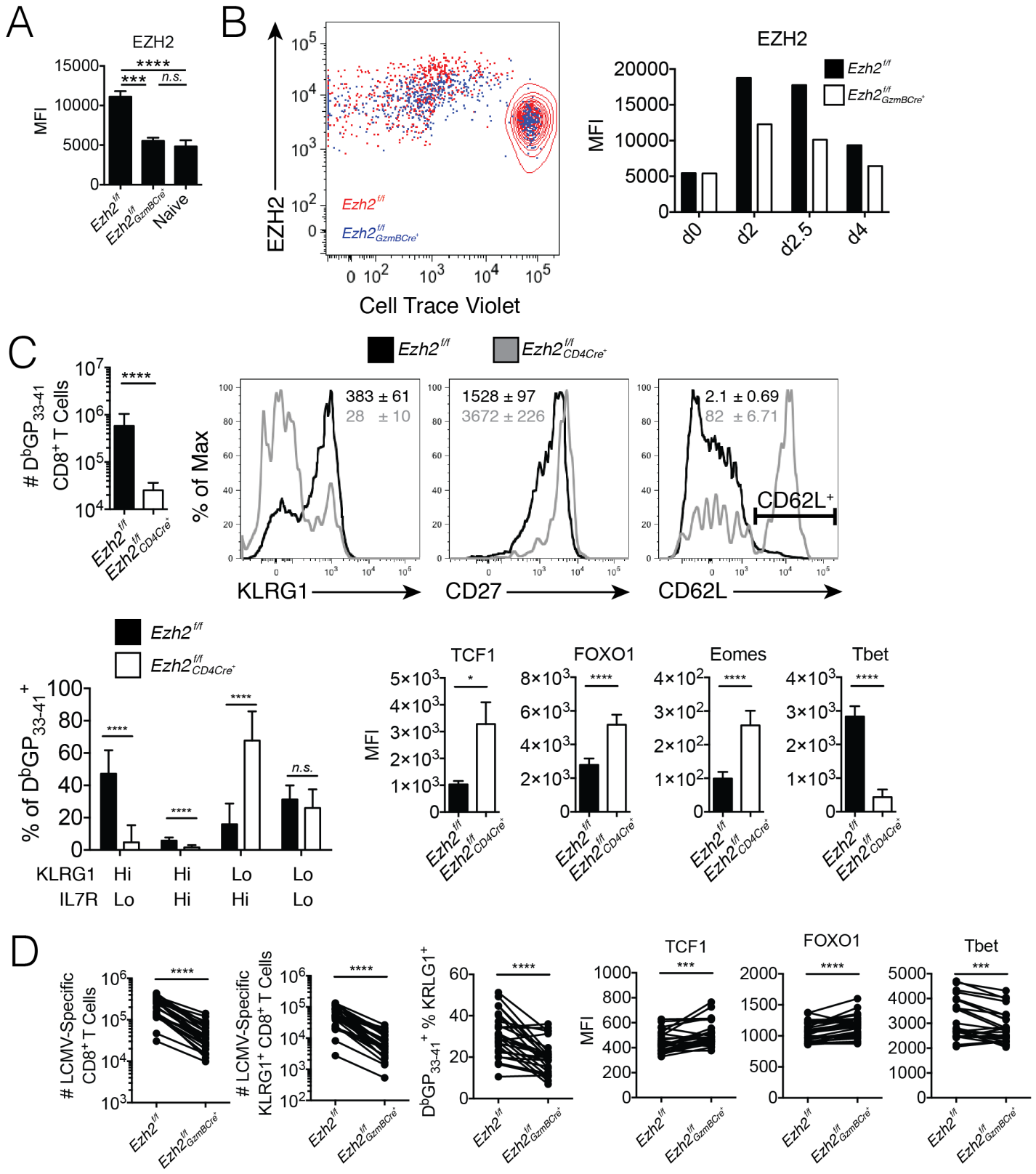

Figure S3. (related to Figure 4) Validation of *Ezh2* deletion characteristics on CD8+ T cell effector development and protein expression.

A) MFI of EZH2 protein level at d4.5 p.i. in virus-specific (D^bGP_{33-41} and $D^bNP_{396-404}$ MHC class I tetramer$^+$) *Ezh2*$^{f/f}$ and *Ezh2*$^{f/f}$ GzmBCre$^+$ CD8$^+$ T cells from the peripheral blood.

B) Congenically mismatched naïve P14$^+$ *Ezh2*$^{f/f}$ (red) and *Ezh2*$^{f/f}$ GzmBCre$^+$ (blue) CD8$^+$ T Cells were pulsed with CellTrace Violet and adoptively co-transferred to the same congenically mismatched WT recipient mouse, which was infected with LCMV Armstrong. Plot shows *in vivo* proliferation of splenic P14$^+$ CD8$^+$ T cells at 60 hrs p.i. P14$^+$ cells from an uninfected recipient are shown as non-divided control. Bar graph shows MFI of EZH2 protein level in splenic P14$^+$ *Ezh2*$^{f/f}$ (solid) and *Ezh2*$^{f/f}$ GzmBCre$^+$ (open) CD8$^+$ T cells at day 0, 2, 2.5, and 4 p.i.

C) *Ezh2*$^{f/f}$ (solid) and *Ezh2*$^{f/f}$ CD4Cre$^+$ (open) mice were infected with LCMV-Armstrong and splenic GP_{33-41}-specific CD8$^+$ T cells were enumerated at d8 p.i; KLRG1, CD27, and CD62L expression were determined at d8 p.i. on splenic GP_{33-41}-specific CD8$^+$ T cells (*Ezh2*$^{f/f}$ is black line, *Ezh2*$^{f/f}$ CD4Cre$^+$ is gray line); the percentage of splenic GP_{33-41}-specific CD8$^+$ T cells in KLRG1/IL7R subsets was determined at d8 p.i.; and the intracellular mean fluorescence intensity (MFI) of the indicated TFs was measured by flow cytometry.

D) Mixed 80% *Ezh2*$^{f/f}$ GzmBCre$^+$ to 20% *Ezh2*$^{f/f}$ bone marrow chimeras (BMC) were infected with LCMV-Armstrong and splenic virus-specific (D^bGP_{33-41} and $D^bNP_{396-404}$ MHC class I tetramer$^+$) CD8$^+$ T cells were examined at d8 p.i. Plots show number of LCMV-specific CD8$^+$ T cells, number of LCMV-specific KLRG1$^+$ CD8$^+$ T cells, percentage of D^bGP_{33-41} tetramer$^+$ CD8$^+$ T cells expressing KLRG1, and MFI of TCF1, FOXO1, and Tbet in splenic D^bGP_{33-41} tetramer$^+$ *Ezh2*$^{f/f}$ and *Ezh2*$^{f/f}$ GzmBCre$^+$ CD8$^+$ T cells paired from the same BMC mouse.

Data shown are representative of two (B) or five (A) independent experiments, or cumulative of three (D) or five (C) independent experiments. Data are expressed as mean ± SD. *p<0.02, ***p<0.001, ****p<0.0001. n=3-5 mice/group/experiment (C-D) or n=4-10 mice/group/experiment (A).

Figure S4. (related to Figure 4)

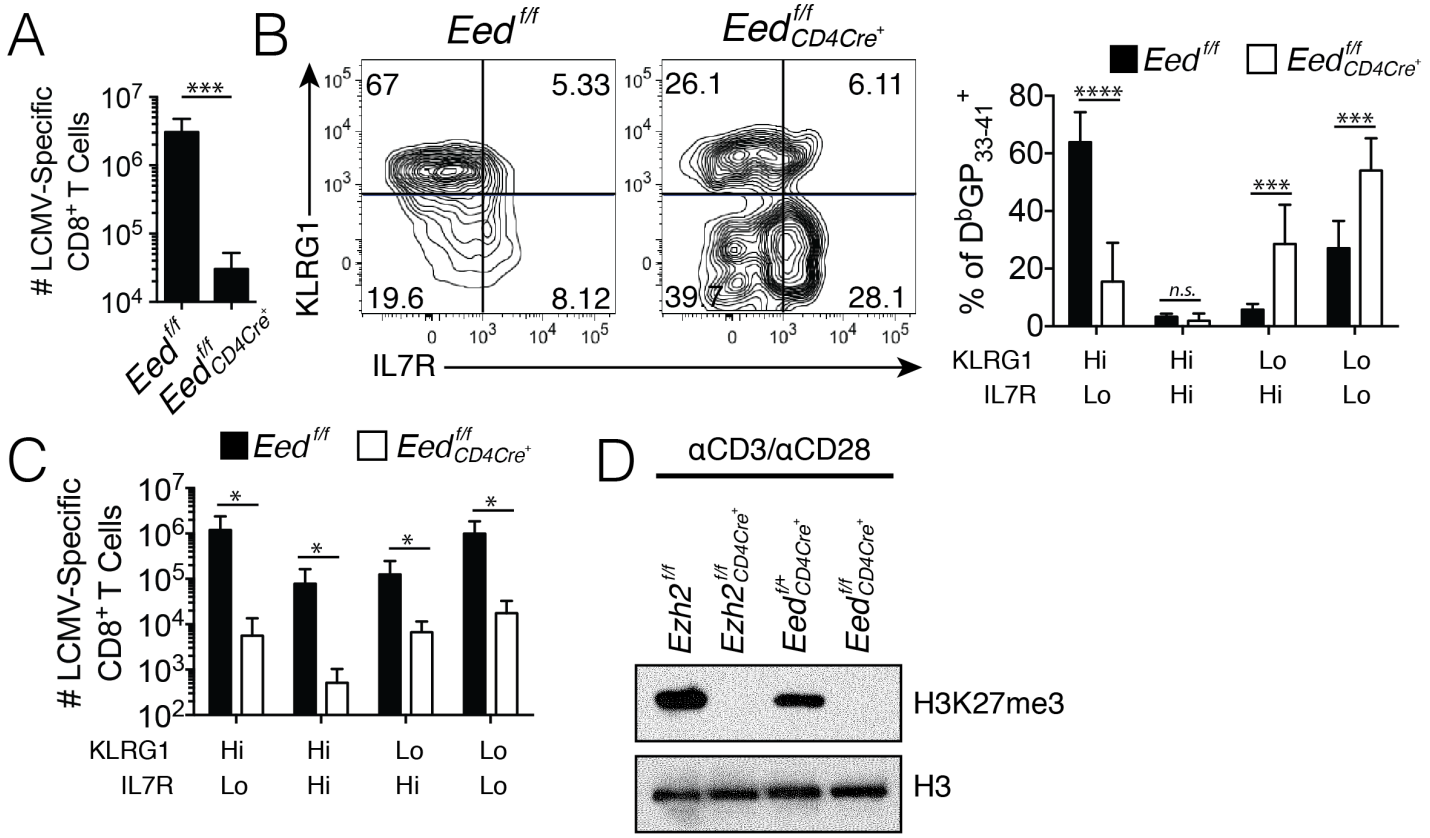

Figure S4. (related to Figure 4) EED deletion is functionally similar to EZH2 deletion day 8 post-infection.

Eed$^{f/f}$ and *Eed*$^{f/f}$CD4Cre^{+} mice were infected with LCMV Armstrong and the number of splenic virus-specific (D^bGP_{33-41} and $D^bNP_{396-404}$ MHC class I tetramer^{+}) CD8^{+} T cells were enumerated at d8 p.i.

B) Contour plots (left) show surface expression of KLRG1 and IL7R on splenic D^bGP_{33-41} tetramer^{+} *Eed*$^{f/f}$ (solid) and *Eed*$^{f/f}$CD4Cre^{+} (open) CD8^{+} T cells from d8 p.i. Bar graph (right) shows average percentages for each subset.

C) Bar graph shows number of splenic virus-specific (D^bGP_{33-41} and $D^bNP_{396-404}$ MHC class I tetramer^{+}) *Eed*$^{f/f}$ (solid) and *Eed*$^{f/f}$CD4Cre^{+} (open) CD8^{+} T cells in KLRG1/IL7R subsets at d8 p.i.

D) *Ezh2*$^{f/f}$, *Ezh2*$^{f/f}$ CD4Cre^{+}, *Eed*$^{f/+}$CD4Cre^{+} and *Eed*$^{f/f}$CD4Cre^{+} CD8^{+} T cells were activated *in vitro* with αCD3 and αCD28 for 3 days, sort purified, and probed for H3K27me3 by western blot.

Data shown are representative of two (D) or cumulative of two (A-C) independent experiments (n=3-5 mice/group/experiment). Data are expressed as mean ± SD. *p<0.05, ***p<0.001, ****p<0.0001

Figure S5. (related to Figure 5)

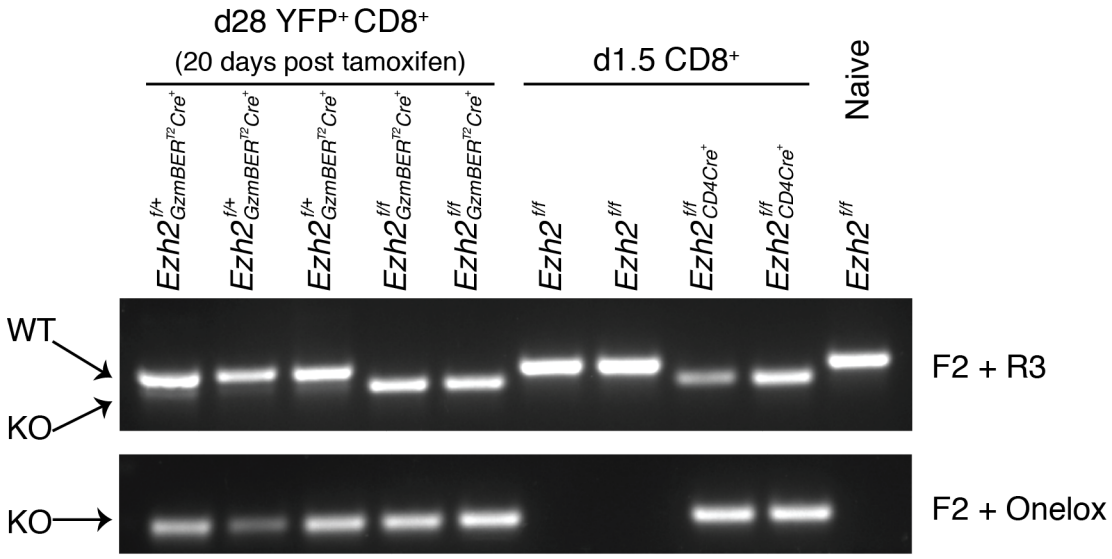

Figure S5. (related to Figure 5) Assessment of EZH2 deletion after completion of tamoxifen treatment in *Ezh2*$^{f/f}$ GzmB-ER^{T2}Cre.

EZH2 deletion was assessed by genomic DNA PCR on *Ezh2*$^{f/+}$GzmBER^{T2}Cre^{+} and *Ezh2*$^{f/f}$GzmBER^{T2}Cre^{+} CD8^{+} T cells purified by FACS at d28 p.i. (20 days after tamoxifen treatment). Purified *Ezh2*$^{f/f}$ and *Ezh2*$^{f/f}$ CD4Cre^{+} CD8^{+} T cells activated *in vitro* for 1.5 days served as a positive control.

Figure S6. (related to Figure 6)

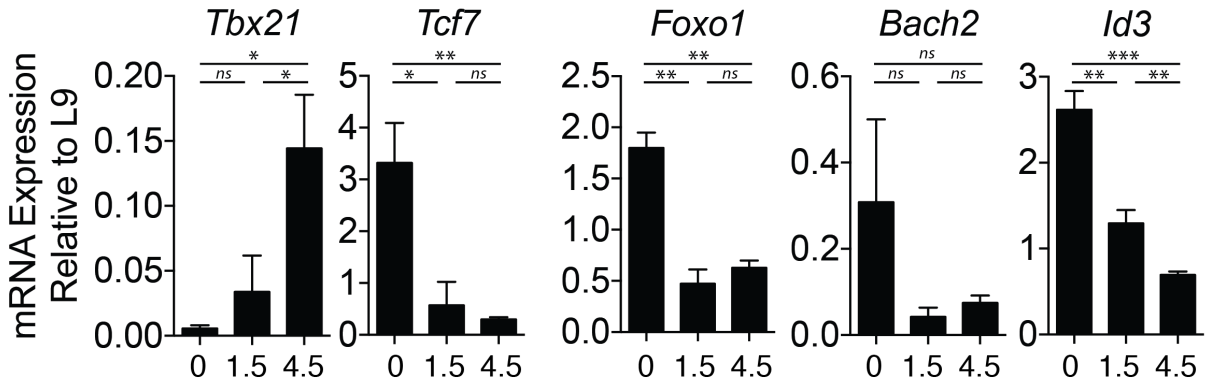

Figure S6. (related to Figure 6) Profiling of mRNA expression in WT CD8$^+$ T cells at early timepoints. A) *Tbx21*, *Tcf7*, *Foxo1*, *Bach2*, and *Id3* mRNA were measured using qRT-PCR in sort purified WT P14$^+$ CD8$^+$ T cells from days 0 (naïve), 1.5, and 4.5 p.i. with LCMV-Armstrong. Data from days 0 and 4.5 p.i. is the same as Fig 6A. Data representative of 3 independent experiments. n=2-3/group/experiment. Data are expressed as mean ± SD. *p<0.05, **p<0.01, ***p<0.001

Figure S7. (related to Figure 7)

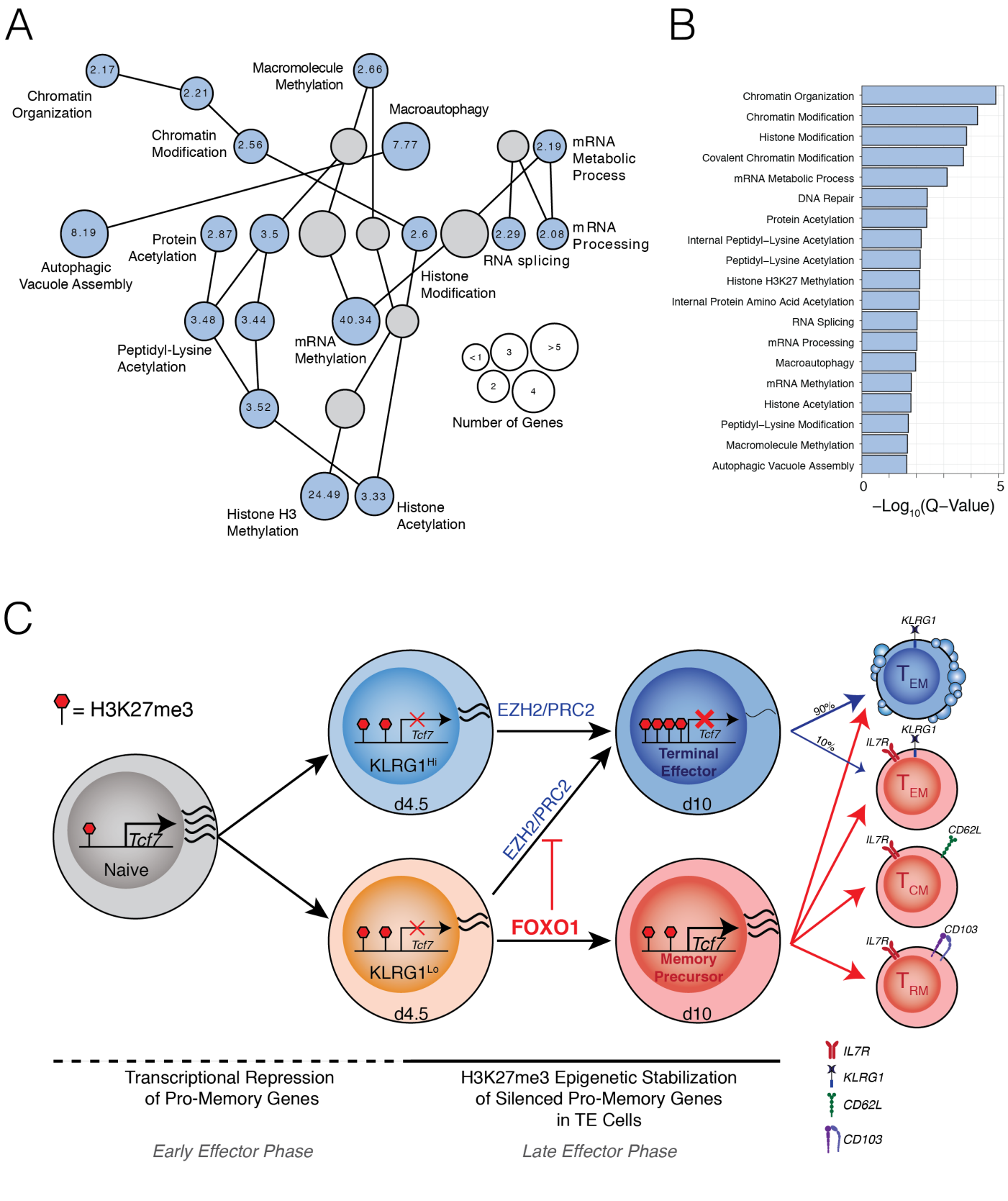

Figure S7. (related to Figure 7) Network analysis of DMRs proximal to FOXO1 binding sites and graphical model.

FOXO1 bound consensus peaks of H3K27ac and H3K27me3 deposition (DMRs and Common) *cis*-regulatory regions were analyzed for the enrichment of biological process ontologies using the Stanford GREAT online resource.

A) Hierarchical-network visualization of enriched biological processes. Significant biological process enrichments with the binomial fold-enrichment shown inside (blue circles); size of the circles denotes the number of regions annotated to the given term.

B) Bar plot showing the $-\log_{10}$(Q-Values) of significantly enriched biological processes (Q-value < 0.05).

C) Graphical model of findings presented in this manuscript.

References

Ahmed, R., Salmi, A., Butler, L. D., Chiller, J. M. & Oldstone, M. B. 1984. Selection of genetic variants of lymphocytic choriomeningitis virus in spleens of persistently infected mice. Role in suppression of cytotoxic T lymphocyte response and viral persistence. *The Journal of Experimental Medicine,* 160**,** 521-540.

Hand, T. W., Morre, M. & Kaech, S. M. 2007. Expression of IL-7 receptor α is necessary but not sufficient for the formation of memory CD8 T cells during viral infection. *Proceedings of the National Academy of Sciences,* 104**,** 11730-11735.

Kaech, S. M. & Ahmed, R. 2001. Memory CD8+ T cell differentiation: initial antigen encounter triggers a developmental program in naive cells. *Nat Immunol,* 2**,** 415-422.

Mackay, L. K., Rahimpour, A., Ma, J. Z., Collins, N., Stock, A. T., Hafon, M. L., Vega-Ramos, J., Lauzurica, P., Mueller, S. N., Stefanovic, T., Tscharke, D. C., Heath, W. R., Inouye, M., Carbone, F. R. & Gebhardt, T. 2013. The developmental pathway for CD103(+)CD8+ tissue-resident memory T cells of skin. *Nat Immunol,* 14**,** 1294-301.

Mclean, C. Y., Bristor, D., Hiller, M., Clarke, S. L., Schaar, B. T., Lowe, C. B., Wenger, A. M. & Bejerano, G. 2010. GREAT improves functional interpretation of cis-regulatory regions. *Nat Biotechnol,* 28**,** 495-501.

Murali-Krishna, K., Altman, J. D., Suresh, M., Sourdive, D. J., Zajac, A. J., Miller, J. D., Slansky, J. & Ahmed, R. 1998. Counting antigen-specific CD8 T cells: a reevaluation of bystander activation during viral infection. *Immunity,* 8**,** 177-87.

Szabo, S. J., Kim, S. T., Costa, G. L., Zhang, X., Fathman, C. G. & Glimcher, L. H. 2000. A novel transcription factor, T-bet, directs Th1 lineage commitment. *Cell,* 100**,** 655-69.